EXPLORING THE LIMITS OF THE DIPOLE APPROXIMATION WITH ANGLE-RESOLVED ELECTRON TIME-OF-FLIGHT SPECTROMETRY

Sierra Laidman,[A] Monica Pangilinan,[B] Renaud Guillemin,[C,D] Sung Woo Yu,[C,D] Gunnar Öhrwall,[C,D] Dennis Lindle,[C] and Oliver Hemmers[C]

ABSTRACT

Understanding the electronic structure of atoms and molecules is fundamental in determining their basic properties as well as the interactions that occur with different particles such as light. One such interaction is single photoionization; a process in which a photon collides with an atom or molecule and an electron with a certain kinetic energy is emitted, leaving behind a residual ion. Theoretical models of electronic structures use the dipole approximation to simplify x-ray interactions by assuming that the electromagnetic field of the radiation, expressed as a Taylor-series expansion, can be simplified by using only the first term. It has been known for some time that the dipole approximation becomes inaccurate at high photon energies, but the threshold at which this discrepancy begins is ambiguous. In order to enhance our understanding of these limitations, we measured the electron emissions of nitrogen. Beamline 8.0.1 at the Advanced Light Source was used with an electron Time-of-Flight (TOF) end station, which measures the time required for electrons emitted to travel a fixed distance. Data were collected over a broad range of photon energies (413 - 664 eV) using five analyzers rotated to 15 chamber angles. Preliminary analysis indicates that these results confirm the breakdown of the dipole approximation at photon energies well below 1 keV and that this breakdown is greatly enhanced in molecules just above the core-level ionization threshold. As a result, new theoretical models must be made that use higher order terms that were previously truncated.

INTRODUCTION

Quantum mechanics is used to describe particles on the atomic scale. Quantum mechanics uses wave functions describing electrons in a field of a nucleus. In case of photoionization, wave functions are used to describe discrete orbitals and the emission of photo- or Auger electrons. The famous time-dependent Schrödinger equation is used to find solutions for a given Hamiltonian (the interaction operator) between the bound state and the continuum state. A photon colliding with an atom transfers angular momentum to the outgoing electron during the photoionization process. This free electron can be described by a wave function as a plane wave that is comprised of spherical waves ($e^{i\mathbf{kr}}$). With the help of a Taylor series expansion for $e^{i\mathbf{kr}}$ it is possible to separate the contributions from the spherical waves. If all contributions except for the first ($e^{i\mathbf{kr}}=1$) are truncated, it is termed the Dipole Approximation (DA).

The interaction of x-rays with an atom or molecule is used to probe its electronic structure and the dynamic behavior during photoionization. Using the dipole approximation simplifies theoretical models and neglects all effects resulting from higher-order momenta. As a result, the limits of the dipole approximation must be investigated in order to have more accurate models.[1]

For over three decades nobody had serious doubts about the validity of the DA. In the UV and far-UV photon-energy ranges, the DA for photoionization is grounded in solid physical reasoning. This is because photoelectron velocities following photoemission are extremely small compared to the speed of light, and the wavelength of the light is much larger than the orbitals of the ejected electrons.[2] However, it is widely known that the dipole approximation breaks down completely at the hard-x-ray energy range ($h\nu > 5$ keV). On the other hand, the breakdown of the dipole approximation at the intermediate soft-x-ray photon-energy range had not been explored until recently. Higher-order multipole moments (electric quadrupole, electric octupole, and magnetic dipole etc.) show some effect at all photon energies. Thus, it is essential to completely understand at what photon energies the dipole approximation can no longer be used and how important the higher-order Taylor series terms are.

The best way to determine these limits is by measuring the angular distributions of photoelectrons because these are much more sensitive to higher-order effects than the partial cross sections. Electron Time-of-Flight (e-TOF) spectrometry is ideally suited for this task. This technique measures the flight time of electrons between the interaction region and a detector, which

A: Bryn Mawr College, Bryn Mawr, PA; B: Cornell University, Ithaca, NY;
C: University of Nevada, Las Vegas, Las Vegas, NV; D: Lawrence Berkeley National Laboratory, Berkeley, CA

can then be used to calculate not only the kinetic energy of the electrons but also the direction of the emitted photoelectrons.[3] Furthermore, the apparatus is able to measure the entire electron energy spectrum simultaneously, eliminating effects due to time fluctuations in beam intensity and sample pressure.

MATERIALS AND METHODS

The experimental setup used was an electron Time-of-Flight end station, which requires an adequate light source. For this experiment, the Advanced Light Source (ALS) at the Lawrence Berkeley National Laboratory was used. Able to produce light in the x-ray and ultraviolet range with light one billion times brighter than the sun, the ALS offers the light needed to study atoms and molecules.

X-rays are emitted from packets of electrons known as bunches, which each have approximately the same diameter as a human hair. The electrons are accelerated to nearly the speed of light, and their energies are increased inside a booster ring. From there, the electrons enter the storage ring and their energy is ramped up to 1.9 GeV. The electrons, maintaining the same energy, change direction with the help of twelve bending magnets in the storage ring. At these twelve positions the electrons produce light because accelerating charged particles, in this case the electrons, give off electromagnetic radiation. When this radiation is emitted, the electrons lose energy, which must be replenished in order to maintain a constant energy. Radio-frequency cavities, which generate an alternating electromagnetic field, give the electrons the same amount of energy that they lost and allow the electrons to maintain their energy. In addition, more light is produced in straight sections of the ring by insertion devices such as wigglers and undulators. Undulators and wigglers are comprised of a series of magnets that produce a spatially alternating magnetic field. When the electron bunches in the storage ring pass through the undulators or wigglers, the electrons are deflected back and forth, thus increasing the amount of radiation emitted along their flight path. By adjusting the undulator or wiggler gap, the maximum number of photons is produced at the appropriate energy for a chosen photon energy. The difference between undulators and wigglers is that undulators produce light that is coherent and in phase whereas the wiggler light is incoherent.

Most of this radiation, which comes in the form of a broad spectrum ranging from infrared to x-rays, leaves the storage ring by tangential ports into beamlines, which are connected to end stations. In the case of this experiment, beamline 8.0.1 was used with an electron Time-of-Flight end station. This end station requires that the ALS operates in 2-bunch mode instead of multibunch mode. The length of each bunch in 2-bunch mode is, on average, 50 picoseconds and the time separation between these two bunches is 328 nanoseconds.

Once the light enters the beamline, a monochromator is used to select a specific wavelength (and thus a specific energy) of photons. In order to do this, a grating diffracts the radiation and a specific wavelength is selected by the exit slit. The monochromator on beamline 8.0.1 has three spherical gratings with radii of 70 m. Each grating is suitable for a different energy range, which is determined by its coating and the number of lines per millimeter.

Various optical devices, such as the entrance and exit slits, are used along the beamline in order to focus, bend, and control the incoming photons. The entrance and exit slits can be varied in slit width and are used in order to adjust the resolution of the monochromator. Directly before the entrance slit, the Vertical Condensing Mirror serves to reduce the height of the beam so that more photons will pass through the entrance slit. Beyond the exit slit, Horizontal and Vertical Refocusing Mirrors are aligned perpendicular to each other in order to achieve maximum horizontal and vertical focusing (Figure 1).

From the beamline, the light enters the vacuum chamber of the electron Time-of-Flight end station (Figure 2). This chamber supports the analyzers and can be rotated about the x-ray beam by 90 degrees while under vacuum. This allows the collection of spectra at many different angles, increasing the accuracy of angular-distribution measurements and allowing for the calculation of additional angular-distribution parameters.

Photons interact with gas that is ejected perpendicular to the photon beam by a needle in a space called the interaction region. There, photoemission occurs due to the collision of the photons from the beam and the gas particles. These electrons can go into an analyzer and must travel a distance of 437.5 mm

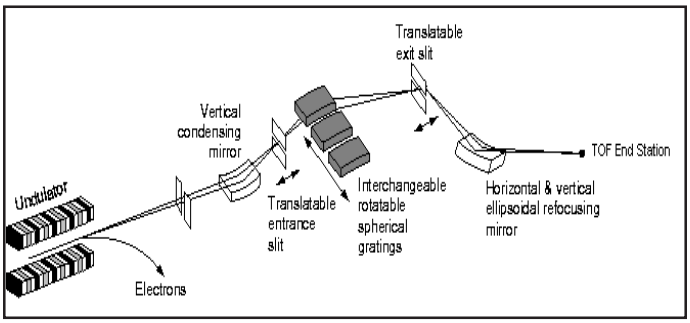

Figure 1. Schematic diagram of Beamline 8.0.1

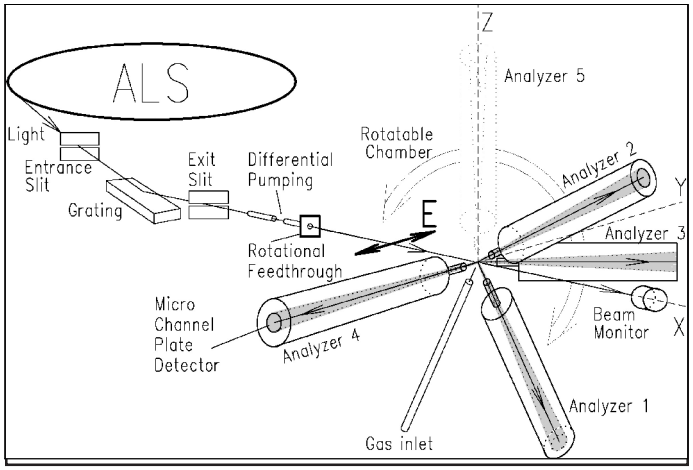

Figure 2. Experimental schematic of the electron Time-of-Flight system. Light from the ALS storage ring passes through beamline optics into a differential-pumping section. The chamber and analyzers can rotate around the photon beam for more accurate electron angular-distribution measurement.

and be within a ± 2.7 degrees cone relative to a straight flight path in order to be detected.

Electrons have to have a minimum kinetic energy of 5 eV to arrive at the detector of any analyzer within the 328 ns time window. Analyzers 2 and 3 are positioned on a cone with a half angle of 54.7 degrees along the photon beam and out of the plane perpendicular to the x-ray beam. For a certain chamber position analyzers 1 and 3 are at the so-called "magic angle." This is the angle at which the dipole parameter disappears from the equation of the differential partial cross section, leaving behind the nondipole parameters. Positioning the analyzers at the "magic angle" allows only nondipolar angular-distribution effects to be studied. Analyzers 1, 4, and 5 are used to measure dipolar angular distributions and cross-section ratios.

Once inside an analyzer, the electrons are detected by two Micro-Channel Plates (MCPs) positioned in a Chevron arrangement. MCPs are thin glass disks with thousands of microscopic tubes. A high voltage is applied across the MCPs and when electrons collide with the walls of the tubes, they produce secondary electrons, which accelerate and cascade down the tubes thus creating even more electrons.

After an electron hits the Micro-Channel Plates, a cloud of electrons is made that hits an anode which charges a capacitor that produces a main pulse each time it discharges. From there, this pulse is amplified. A Constant Fraction Discriminator then inverts the signal, shifts it by less than a nanosecond, and adds the original signal to the inverted and shifted signal. This new signal marks the start time for the time-to-amplitude converter/biased amplifier while the end time is marked by the ALS Bunch Marker signal that is produced every 328 ns. The time signal is converted into a voltage using an Analog-to-Digital Converter with the different voltages corresponding to specific channel numbers, which are stored as counts in a Multi-Channel-Analyzer. A spectrum is made up of all the counts produced over all the channel numbers with the peaks in the spectrum corresponding to electrons with certain kinetic energies (Figure 3).

For this experiment, the spectra for molecular nitrogen were collected at fifteen different chamber rotation angles. Nitrogen gas was selected because it is a simple molecule with inner and outer shells, and argon gas was used for calibration purposes further explained in the next section. Nitrogen gas spectra were collected at certain photon energies ranging from 413 eV to 664 eV. Each photon energy required adjustments of the undulator gap for optimal resolution and intensities.

DATA ANALYSIS AND RESULTS

Each analyzer produces a separate spectrum that is used to calculate the differential cross section for photoemission processes. This differential cross section describes the angular distribution of ejected photoelectrons from a randomly oriented sample using 100% linearly polarized light. Using the nondipole parameters (δ and γ which can be combined to the single parameter ζ, equivalent to $\gamma + 3\delta$) and the dipole parameter (β), the equation is as follows:

$$\frac{d\sigma_{nl}}{d\Omega} = \frac{\sigma_{nl}}{4\pi}\left[1 + \frac{\beta}{2}\left(3\cos^2\theta - 1\right) + \left(\delta + \gamma\cos^2\theta\right)\sin\theta\cos\phi\right]$$

Each analyzer has a fixed ϕ and θ (Figure 4) that correspond to the angle of the photoemitted electron in regards to the direction of the photon beam and its polarization. σ_{nl} corresponds to the partial cross section of electrons from subshells *nl*. The equations relating to analyzers 1, 3, and 4 are the only ones needed in order to obtain the dipole and nondipole parameters (β, ζ respectively) (Figure 5).

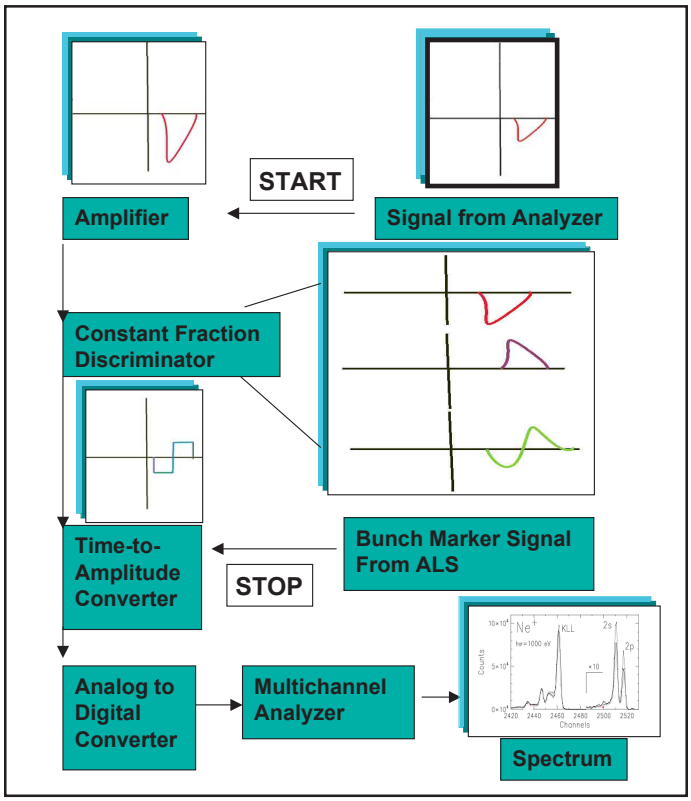

Figure 3. Flow chart of how the signal given by an electron becomes part of a spectrum.

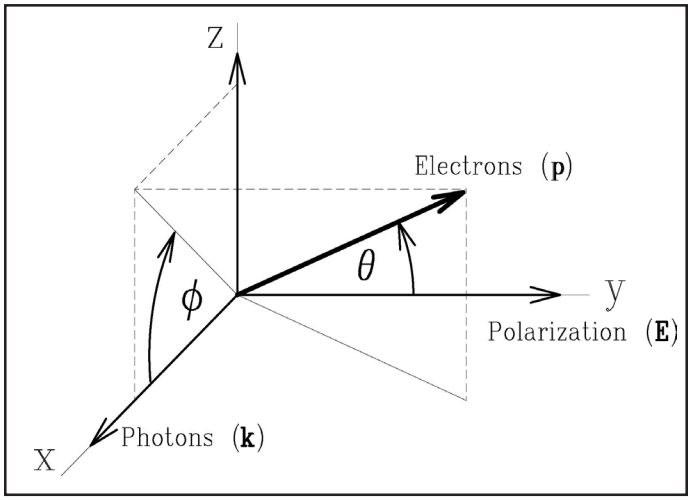

Figure 4. The coordinate system and angles used for the experiment.

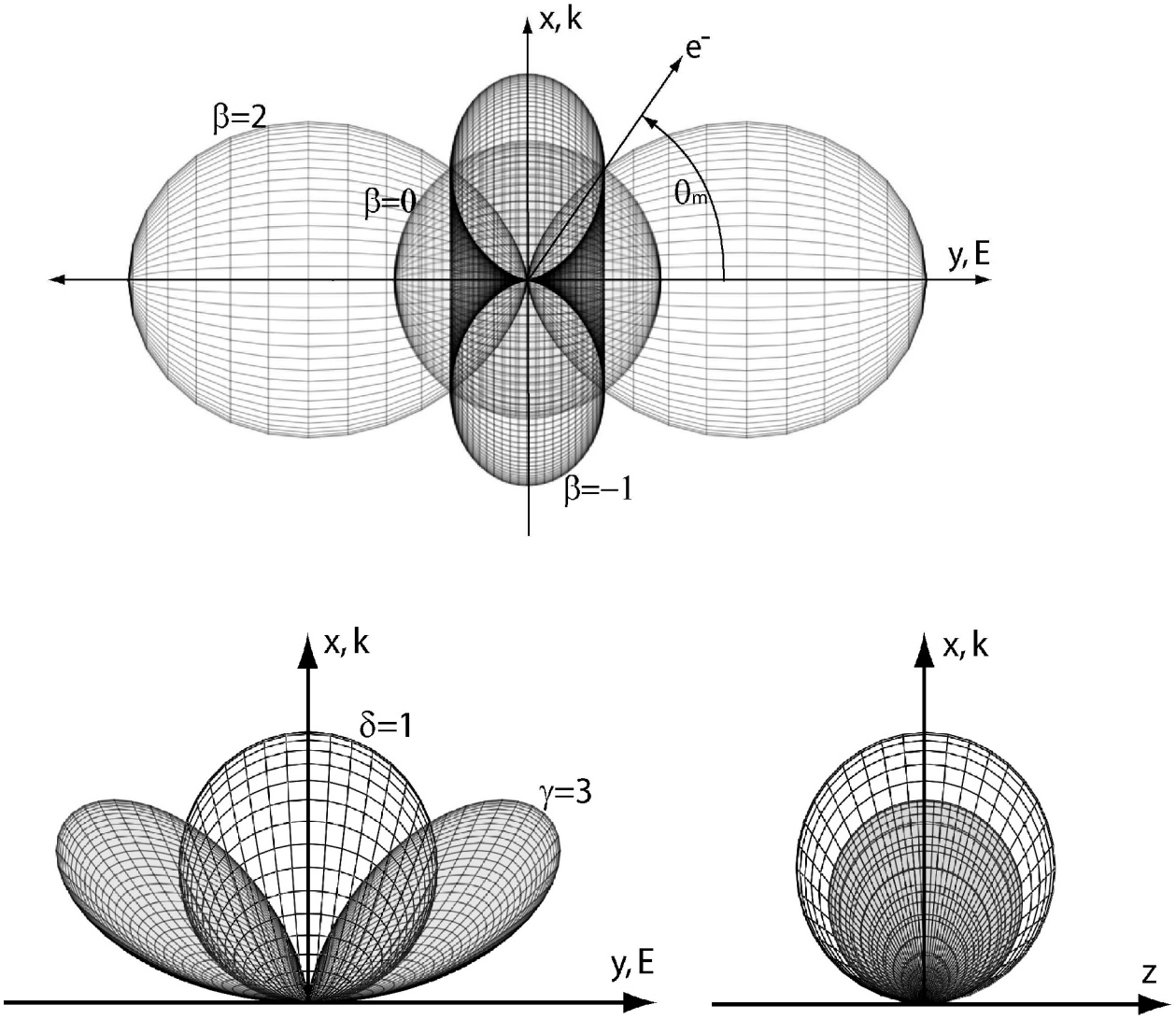

Figure 5. Top - Angular distribution pattern for the dipole parameter β. As β changes values, the angular distribution pattern changes shape. Bottom - The nondipole angular distrubution describing δ and γ. Unlike the dipole angular distrubution pattern, as δ and γ change values, the pattern are scaled accordingly.

$$A_{analyzer\ number}(\theta,\ \phi) = Area$$

$$T_{analyzer\ number} = Electronic\ and\ Detector\ Efficiencies$$

$$A_1(54.7^\circ, 90^\circ) = \frac{d\sigma}{d\Omega} = \frac{\sigma}{4\pi} T_1$$

$$A_3(54.7^\circ,\ 0^\circ) = \frac{d\sigma}{d\Omega} = \frac{\sigma}{4\pi}\left(1+\sqrt{\frac{2}{27}}\zeta\right) T_3$$

$$A_4(0^\circ, 90^\circ) = \frac{d\sigma}{d\Omega} = \frac{\sigma}{4\pi}(1+\beta) T_4$$

The differential cross section is proportional to the area under the N 1*s* peak for nitrogen gas (Figure 6). By dividing the differential cross sections for analyzers 3 and 4 by that for analyzer 1, it is possible to determine the angular distribution parameters without knowing the partial photoionization cross section.

$$\beta = \left(\frac{T_1}{T_4}\frac{A_4}{A_1}\right) - 1$$

$$\zeta = 3\delta + \gamma = \sqrt{\frac{27}{2}}\left(\frac{T_1}{T_3}\ \frac{A_3}{A_1} - 1\right)$$

Argon gas was used for calibration because all of the dipole and nondipole parameters are known for this element. This way we determine the efficiencies for each analyzer pair.

$$\frac{T_1}{T_4} = (\beta_{Ar} + 1)\frac{A_{1Ar}}{A_{4Ar}}$$

$$\frac{T_1}{T_3} = \left(\sqrt{\frac{27}{2}}\zeta_{Ar} + 1\right)\frac{A_{1Ar}}{A_{3Ar}}$$

Now that all the necessary parameters are known, the nondipole and dipole parameters can be determined for that particular energy. Each of these equations must be solved for each spectrum and from there a graph can be made of the nondipole or dipole parameter over the photon energy.

DISCUSSION AND CONCLUSIONS

Figure 7 shows experimental data of the N_2 N 1*s* nondipole parameter ζ as filled circles with error bars and theoretical data for molecular nitrogen as a solid line that is in excellent agreement with the data points. The theory for atomic nitrogen is shown as a dot-dashed line. The broad peak centered at about 470 eV photon energy is due to significant contributions of the nondipole parameters in Equation 1.

The theory for atomic nitrogen lacks the resonance-like feature seen in the experimental data, leading to the conclusion that this behavior has a molecular origin despite the largely atomic-like nature of the occupied 1*s* orbitals in molecular nitrogen. The theory for molecular nitrogen is explained in detail elsewhere.[5]

In short, the magnitude of nondipole effects is dependent on the relation between the photon energy and the size of the orbital. When the photon has a larger wavelength (which corresponds to a lower photon energy) than the orbital, the nondipole effect is small. On the other hand, if the orbital is larger than the photon wavelength, the nondipole effect is large. When comparing N_2 N 1*s* ionization with atomic nitrogen N 1*s* ionization, the nondipole effect is more pronounced in molecular nitrogen. This is rather puzzling because the N 1*s* orbitals are about the same size. Based on theoretical calculations these larger nondipole effects depend on the bond-length distance between the two nitrogen atoms. Therefore, it is necessary to also include the comparison between the wavelength and the bond-length. It has been shown that the nondipole effect is related to the bond-length size to a larger extent than the orbital size and some other molecular contributions.[5] Theory starts to deviate at lower photon energies (410-420 eV). This deviation is attributed to the fact that the theory uses a frozen-core approximation for the calculations and a dynamical potential change needs to be implemented. The observed nondipole effects appear to indicate a universal nondipole characteristic in molecular photoionization, which demands further experimental and theoretical study.

ACKNOWLEDGEMENTS

We would like to thank the United States Department of Energy, Office of Science for giving us the opportunity to participate in the Energy Research Undergraduate Laboratory Fellowship (ERULF). Our appreciation also goes out to the entire staff at the Advanced Light Source and the Lawrence Berkeley National Laboratory. We would like to thank our mentor, Fred Schlachter, for providing us with data to analyze and experiments to help run. The ALS is funded by the Department of Energy, Materials Sciences Division, and Basic Energy Sciences under Contract No. DE-AC03-76SF00098.

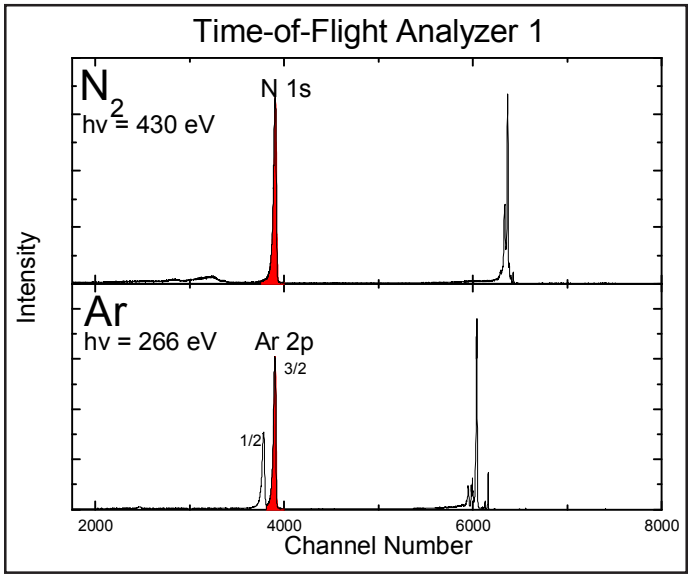

Figure 6. Spectra of nitrogen and argon at a certain photon energy. The colored sections under the graphs indicate which areas were used to calculate the dipole and nondipole parameters.

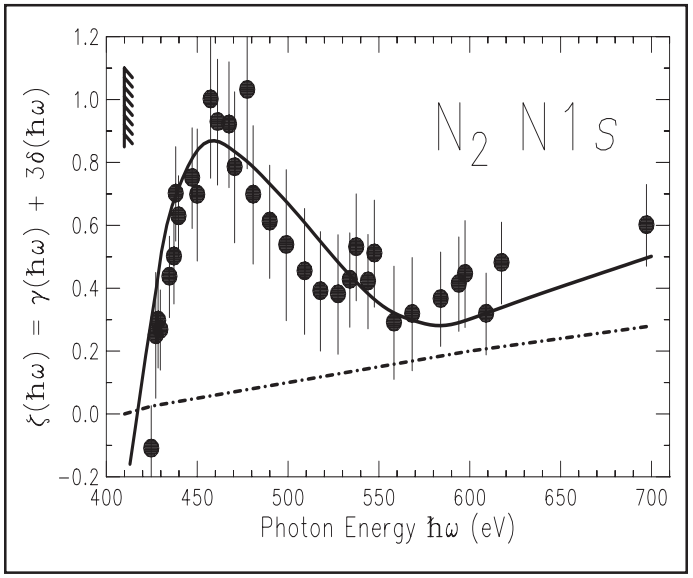

Figure 7. Nondipole parameter ζ for molecular nitrogen. The filled circles with error bars are the data collected as described in the text. The theory for molecular nitrogen is the solid line and the theory for atomic nitrogen is the dot-dashed line.

REFERENCES

1 Derevianko, A., Hemmers, O., Oblad, S., Glans, P., Wang, H., Whitfield, S.B., Wehlitz, R., Sellin, I.A., Johnson, W.R., and Lindle, D.W., "Electric-Octupole and Pure-Electric-Quadrupole Effects in Soft-X-Ray Photoemission," Phys. Rev. Lett. 84, 2116 (2000).

2 Lindle, D. W., Hemmers, O. A. (2000). "Time-of-Flight Photoelectron Spectroscopy of Atoms and Molecules," Proc. of Pan American Advanced Studies Institute. Angra dos Reis, Brazil, April 27 — May 7, 2000 edited by C. Cisneros, H. Bryant, and F. Schlachter.

3 Hemmers, O.A., Lindle, D.W. (2000). "Non-dipolar Effects in Soft-x-ray Photoemission," Proc. of Pan American Advanced Studies Institute. Angra dos Reis, Brazil, April 27 — May 7, 2000 edited by C. Cisneros, H. Bryant, and F. Schlachter.

4 Hemmers, O.A., Whitfield, S.B., Glans, P., Wang, H., Lindle, D.W., Wehlitz, R., and Sellin, I.A., "High-resolution Electron Time-of-Flight Apparatus for the Soft X-ray Region" Review of Scientific Instruments, vol. 69, November 1998. 3809-3817.

5 Hemmers, O.A., Wang, H., Focke, P., Sellin, I.A., Lindle, D.W., Arce, J.C., Sheehy, J.A., Langhoff, P.W., "Large Nondipole Effects in the Angular Distribution of K-Shell Photoelectrons from Molecular Nitrogen", Phys. Rev. Lett. 87, 273003 (2001).